Magnetostatic Spring Softening and Stiffening in Magneto-Mechanical Resonator Systems

Inbar Hotzen Grinberg[1], Anudeep Mangu[2], Christopher W. Peterson[3], Eli Wilken-Resman[3], Jennifer T. Bernhard[3], and Gaurav Bahl[1]

[1]Department of Mechanical Science and Engineering, University of Illinois at Urbana–Champaign, Urbana, IL 61801 USA
[2]Department of Physics, University of Illinois at Urbana–Champaign, Urbana, IL 61801 USA
[3]Department of Electrical and Computer Engineering, University of Illinois at Urbana–Champaign, Urbana, IL 61801 USA

Integrating magnets into resonant mechanical systems allows for intriguing capabilities, such as the ability to tune the mechanical resonance frequency or induce coupling between resonators without any physical contact. Here, we present analytical models as well as the experimental study of an integrated magneto-mechanical system. Using a point dipole approximation, we explore the magneto-static spring effect, which can either soften or stiffen a spring depending on dipole orientation and spatial position of the magnets. We use translational and rotational resonance as commonly encountered demonstrative cases and, experimentally, demonstrate both the spring softening and stiffening effects.

Index Terms—**Magneto-mechanics, nonlinear dynamics, spring softening, spring stiffening.**

I. Introduction

FORCES that exhibit a linear dependence on the position of a moving object produce an effect equivalent to a mechanical spring and can tune the natural frequency of a mechanical oscillator. This effect is responsible for well-known phenomena such as electrostatic spring softening in MEMS [1], [2] and atomic force microscopes [3], [4], as well as the optical spring effect due to radiation-induced forces in optomechanical systems [5], [6]. Magnetically sensitive mechanical oscillators within nonuniform magnetic fields can also experience a magnetostatic spring effect, which is the basis of magnetic force microscopy [7], [8]. As magneto-mechanical systems become increasingly relevant for energy harvesting [9]–[11], sensors [12]–[14], actuators [15]–[17], and metamaterials [18]–[20], understanding of this spring effect becomes increasingly important. The magnetic spring formed by concentric rings was investigated in [21]–[23], whereas [24]–[27] focused on the nonlinear magnetic interaction and close proximity forces. Here, we focus on a regime where the magnetic interaction can be characterized by a point dipole approximation and is dominated by linear behavior.

In this paper, we investigate the magnetostatic spring effect in the context of magneto-mechanical oscillators undergoing both translational and rotational resonances. We show that the magnetostatic spring can either soften or stiffen an oscillator depending on spatial location as well as vector orientation of the dipole. This richness of behavior can also impact the magnetically induced coupling within oscillator arrays and can uniquely generate both positive and negative inter-oscillator coupling rates.

Manuscript received January 16, 2019; revised March 6, 2019; accepted March 15, 2019. Date of publication April 25, 2019; date of current version July 18, 2019. Corresponding author: I. H. Grinberg (e-mail: inbar28@illinois.edu).

This paper has supplementary downloadable material available at http://ieeexplore.ieee.org, provided by the author.

Color versions of one or more of the figures in this paper are available online at http://ieeexplore.ieee.org.

Digital Object Identifier 10.1109/TMAG.2019.2906864

II. Magnetostatic Spring Effect

For this paper, we select a simple two-magnet system, each of which is allowed the same oscillatory degree of freedom (DOF)—either translational or rotational—with the assistance of restoring mechanical springs. Each magnet is a source of a nonuniform magnetic field that influences the dynamics of the other magnet. This arrangement is selected as it provides a simple canonical example and yet demonstrates the complexity of the magnetostatic spring effect. The methods and inferences in this paper can readily be extended to more complex systems composed of several magnetic oscillators and more complex spatial field dependences. To simplify the analysis, we treat the two magnets as point dipoles, which is heuristically acceptable as long as the distance between them is greater than their largest geometrical dimension. Generally, a magnetic dipole $\vec{m}$ in a magnetic field $\vec{B}$ feels a force $\vec{F} = \nabla(\vec{m} \cdot \vec{B})$ and a torque $\vec{\tau} = \vec{m} \times \vec{B}$, both depending on the orientation and position of the dipole within the field. The magnetic field produced by a point dipole is given by $\vec{B} = (3(\vec{m} \cdot \vec{r})\vec{r} - r^2\vec{m})\mu_0/4\pi r^5$. Therefore, for a two-magnet system, the torque and force acting on magnet 1 due to magnet 2 take the forms

$$\vec{\tau}_{12} = \frac{\mu_0}{4\pi r^5}(3\vec{m}_2 \times (\vec{m}_1 \cdot \vec{r})\vec{r} - r^2(\vec{m}_2 \times \vec{m}_1)) \tag{1}$$

and

$$\vec{F}_{12} = \frac{3\mu_0}{4\pi r^4}(\vec{m}_2(\vec{m}_1 \cdot \hat{r}) + \vec{m}_1(\vec{m}_2 \cdot \hat{r}) + \hat{r}(\vec{m}_1 \cdot \vec{m}_2) - 5\hat{r}(\vec{m}_1 \cdot \hat{r})(\vec{m}_2 \cdot \hat{r})). \tag{2}$$

Here, $\mu_0 = 4\pi \times 10^{-7}\ N/A^2$ is the magnetic permeability of free space, $\hat{r}$ is a unit vector in the direction of $\vec{r} = x\hat{x} + y\hat{y} + z\hat{z}$, which is the position of magnet 2 relative to magnet 1, and

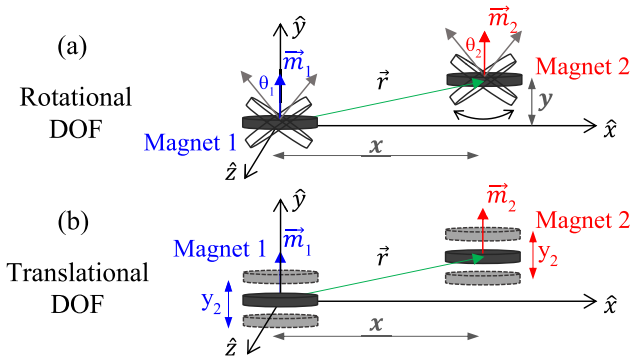

Fig. 1. Schematic of a two-magnet system, $\vec{m}_1$ and $\vec{m}_2$ are the dipole moments, and $\vec{r}$ is their relative position vector. (a) Rotational DOF of the magnets around $\hat{z}$. (b) Translational DOF of the magnets along $\hat{y}$.

$\vec{m}_1, \vec{m}_2$ are the two magnetic dipoles. We separate our analysis into two cases: 1) rotational resonance around $\hat{z}$ [Fig. 1(a)] to analyze the spring contribution from the magnetic torque and 2) translational resonance along $\hat{y}$ [Fig. 1(b)] to analyze the spring contribution of the magnetic force. For both cases, the dipoles are assumed to be oriented along $\hat{y}$ at rest.

We first analyze the rotational resonance case shown in Fig. 1(a). Assuming that the angular amplitude is small, the magnetostatic torque acting on magnet 1 oriented along unit vector $\hat{z}$ is given by

$$\tau_{12}(\theta_1, \theta_2) = \frac{\mu_0 m_1 m_2}{4\pi r^5}((x^2 - 2y^2)\theta_1 + (2x^2 - y^2)\theta_2 - 3xy) \quad (3)$$

where θ_1 and θ_2 are the angles of rotation of magnets 1 and 2, respectively. The equation of motion for magnet 1 can then be written as

$$I\ddot{\theta_1} + c\dot{\theta_1} + \kappa\theta_1 = \tau_{12}(\theta_1, \theta_2) \quad (4)$$

where I is the cross-sectional moment of inertia, κ represents the torsional mechanical restoring spring constant, and c is the viscous damping coefficient. In this paper, we do not consider the effects of dry friction [28]. Since $\tau_{12} \neq 0$ for $\theta_1 = \theta_2 = 0$, the system is not at equilibrium for zero deflections, and to obtain the magnetic effect, we must linearize the system around the new equilibrium deflections $\theta_{\text{eq},1}, \theta_{\text{eq},2}$. However, by assuming small magnetic interaction or large mechanical stiffness, this equilibrium can be neglected (a full derivation without this assumption is provided in the Appendix). This allows substitution of (3) into (4) to produce the linearized equation of motion

$$\ddot{\theta_1} + \tilde{c}\dot{\theta_1} + (\omega_0^2 - \tilde{\gamma})\theta_1 - \tilde{\alpha}\theta_2 = 0 \quad (5)$$

where

$$\tilde{c} = \frac{c}{I}\ ;\ \omega_0^2 = \frac{\kappa}{I}\ ;\ \tilde{\gamma} = \frac{\gamma}{I}\ ;\ \gamma = \frac{\mu_0 m_1 m_2}{4\pi r^3}\frac{x^2 - 2y^2}{r^2}$$
$$\tilde{\alpha} = \frac{\alpha}{I}\ ;\ \alpha = \frac{\mu_0 m_1 m_2}{4\pi r^3}\frac{2x^2 - y^2}{r^2}\ ;\ r = |\vec{r}|. \quad (6)$$

From (5), we see that the coefficient $\tilde{\gamma}$ acts as an additional spring term and $\tilde{\alpha}$ is a coupling coefficient between the two magnets. These coefficients can take on either positive or negative values and can, therefore, introduce either a spring softening or stiffening effect as well as either negative or positive coupling between the resonators. Fig. 2(a) presents a computed 2-D map of the rotational magnetostatic spring effect due to γ with respect to the purely geometrical coordinates x and y.

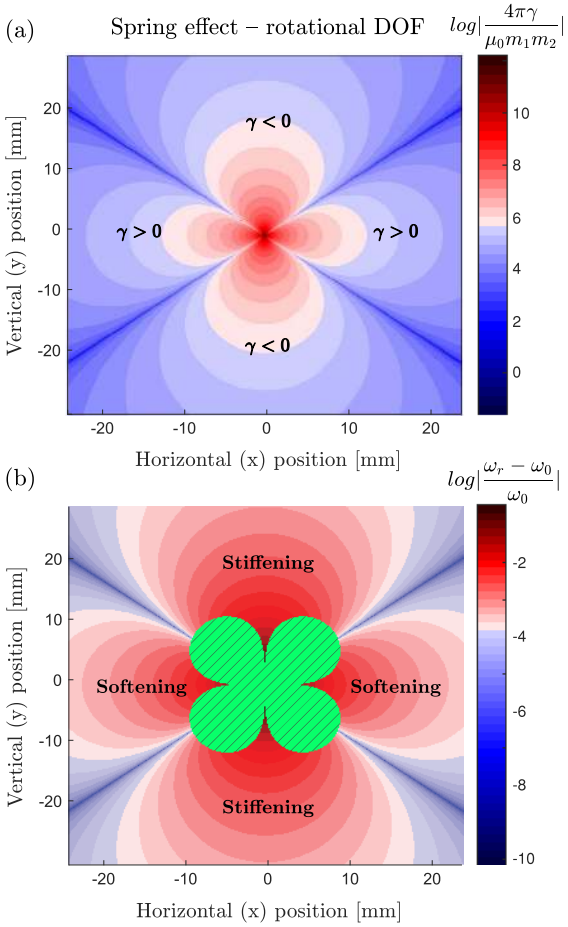

Fig. 2. Calculated magnetostatic spring effect for a system with a rotational DOF. (a) Color map of normalized γ [the spring modification parameter given in (6)] as a function of the relative position in x and y of two magnets. (b) Fractional frequency shift calculated for specific values of μ_0, m_i, κ based on our experiments. Striped green area marks where $\theta_{\text{eq,i}} > 10^{-2}$ and our linearized approximation does not hold (see the Appendix).

We can also write the fractional shift of the natural frequency as $(\omega_r - \omega_0)/\omega_0 = (1 - \gamma/\kappa)^{(1/2)} - 1$, where $\omega_r = (\omega_0^2 - \tilde{\gamma})^{(1/2)}$ is the new resonance frequency. Fig. 2(b) presents the 2-D spatial variation of this fractional frequency shift evaluated for the position independent pre-factor $\mu_0\ m_1\ m_2/4\pi\kappa = 1.5 \cdot 10^{-8}\ 1/m^3$, corresponding to the experimental measurements discussed later in this paper. Since we are assigning specific values to the system parameters, the assumption of large mechanical stiffness or small magnetic interaction may not be valid, therefore, we include $\theta_{\text{eq,i}}$ in our calculations.

We use a linearized approximation around $\theta_i = 0$ to find $\theta_{\text{eq,i}}$, therefore, the calculated frequency shift is only valid when $\theta_{\text{eq,i}}$ are in the vicinity of the original linearization point (see the Appendix). As a threshold for producing Fig. 2(b), we used $\theta_{\text{eq,i}} < 10^{-2}$.

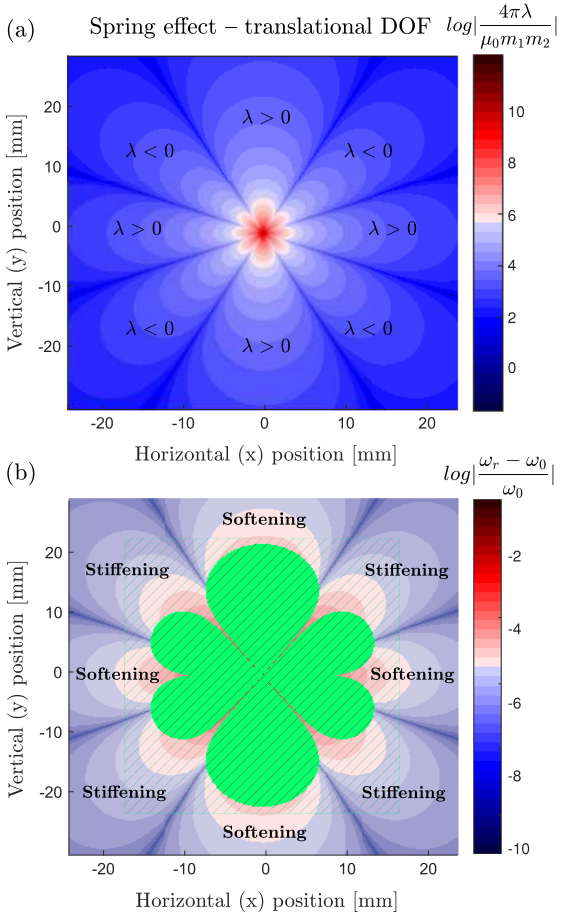

Fig. 3. Calculated magnetostatic spring effect for a system with a translational DOF. (a) Color map of normalized λ (the spring modification parameter) as a function of the relative position in x and y of two magnets (full expression for λ is in the Appendix). (b) Fractional frequency shift plotted for specific values of μ_0, m_i, k based on our experiments. Striped green area marks where $\frac{y_{\text{ieq}}}{r} > 10^{-2}$ and our linearized approximation does not hold (see the Appendix).

We now proceed to analyze the translational system illustrated in Fig. 1(b). The magnetostatic force acting on magnet 1 in the $\hat{y}$ direction is

$$F_{12} = \frac{3\mu_0 m_1 m_2}{4\pi r^5}\left[3(y_0+y_1-y_2) - \frac{5(y_0+y_1-y_2)^3}{r^2}\right] \quad (7)$$

where y_1 and y_2 are the linear displacements of magnets 1 and 2, respectively, and y_0 is the initial spacing between the magnets. As mentioned earlier, there is a non-zero magnetostatic force ($F_{12} \neq 0$ if $y_1 = y_2 = 0$) that may introduce initial deflections $y_{\text{eq},1}, y_{\text{eq},2}$ at equilibrium. However, as in the case of the torque, if the magnetic interaction is assumed to be small, or the mechanical spring constant is assumed to be large, we can reasonably neglect this contribution (a full derivation is in the Appendix). The linearized equation of motion of magnet 1 is then written as

$$\ddot{y_1} + \tilde{c}\dot{y_1} + (\omega_0^2 - \tilde{\lambda})y_1 + \tilde{\lambda}y_2 = \tilde{F_{12}} \quad (8)$$

where

$$\tilde{c} = \frac{c}{M}\ ;\ \omega_0^2 = \frac{k}{M}\ ;\ \tilde{\lambda} = \frac{\lambda}{M}\ ;\ \tilde{F_{12}} = \frac{F_{12}}{M}. \quad (9)$$

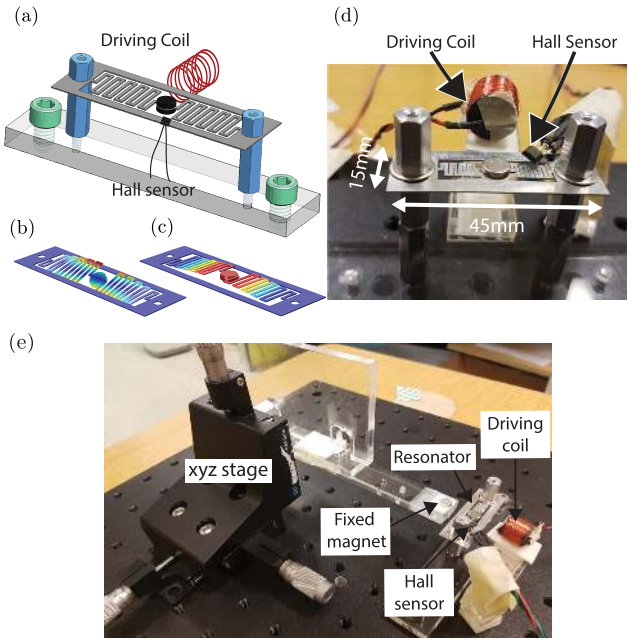

Fig. 4. (a) Illustration of the experimental system comprised of a small magnet mounted on a serpentine mechanical spring. The system is driven to resonance using a coil and deflections are sensed using a Hall sensor. (b) Torsional resonance mode. (c) Bending resonance mode. (d) Photograph of a fabricated device with Hall sensor and driving coil. (e) Photograph of the experiment setup including the resonating magnet and the fixed magnet used to induce the spring effect.

Here, M is the mass of the magnet, k is the mechanical spring constant, c is a damping coefficient, and $\lambda = (\partial F_{12})/(\partial y)$ (see the Appendix) functions as both the effective magnetic spring as well as the coupling coefficient between the resonators. Similar to the rotational case, λ can be either positive or negative and, therefore, produce either a softening or a stiffening effect, and either negative or positive coupling. Fig. 3(a) presents a 2-D map of the translational magnetostatic spring effect due to λ with respect to the purely geometrical parameters x and y.

The fractional shift of natural frequency can also be evaluated as $(\omega_r - \omega_0)/\omega_0 = (1 - \lambda/k)^{(1/2)} - 1$, where $\omega_r = (\omega_0^2 - \tilde{\lambda})^{(1/2)}$, and is presented in Fig. 3(b). This plot is evaluated using the position independent pre-factor $\mu_0\ m_1\ m_2/\pi k = 2.5 \times 10^{-11}\ 1/m^3$, corresponding to the experiments shown below. As in the rotational case, since we are assigning specific system parameters we include the equilibrium calculations in this plot. We use linearization around $y_i = 0$ to find $y_{\text{eq,i}}$, therefore, the calculated frequency shift is only valid when $y_{\text{eq,i}}$ are in the vicinity of the original linearization point (see the Appendix). As a threshold for producing Fig. 3(b), we used $(y_{\text{eq,i}})/r < 10^{-2}$.

III. Experimental Results

To experimentally verify our analysis, we fabricated a mechanical resonator with a small neodymium magnet acting as the magnetic mass [Fig. 4(a)]. The serpentine spring structure was cut using wire electrical discharge machining (EDM)

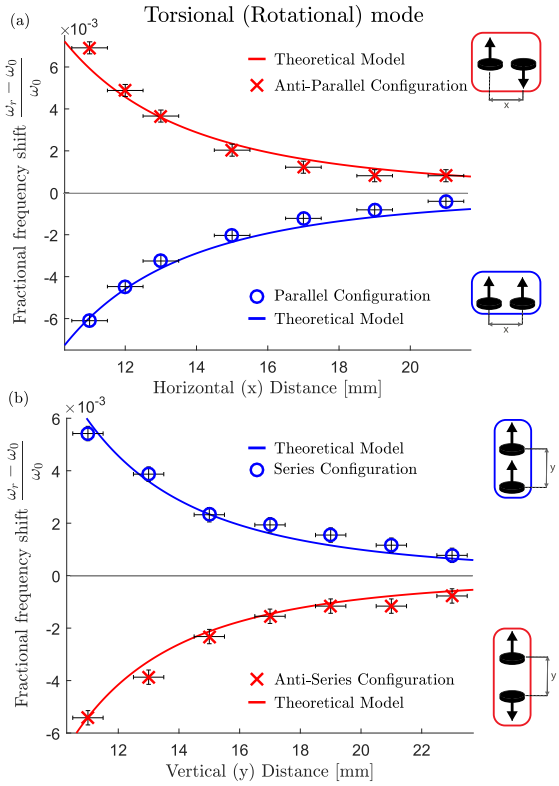

Fig. 5. Measured fractional frequency shift of the torsional resonance as a function of the distance between the resonating magnet and the fixed magnet. (a) Parallel (blue) and anti-parallel (red) arrangements, showing a softening and stiffening effect, respectively. (b) Series (blue) and anti-series (red) arrangements, showing a stiffening and softening effect, respectively. Solid lines: theoretical model predictions.

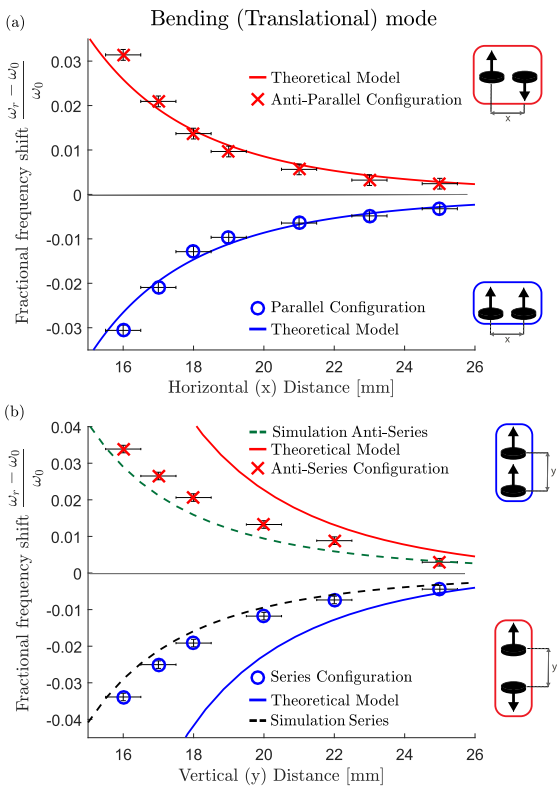

Fig. 6. Measured fractional frequency shift of the translational resonance as a function of the distance between the resonating magnet and the fixed magnet. (a) Parallel (blue) and anti-parallel (red) arrangements, showing a softening and stiffening effect, respectively. (b) Series (blue) and anti-series (red) arrangements showing a softening and stiffening effect, respectively. Solid lines: theoretical model predictions. Dashed lines: predictions based on Ansys Maxwell simulations of the force.

from 0.4-mm-thick aluminum, allowing the structure to support both a torsional (rotational) resonance mode [Fig. 4(b)] and a bending (translational) resonance mode [Fig. 4(c)]. We drive the resonator using a coil that generates a time-varying magnetic field and measure the motion of the magnet using a Hall sensor [Fig. 4(d)]. The amplitude of the magnetic field produced by the coil is experimentally confirmed to be at least an order of magnitude smaller than the field produced by the resonating magnet. In addition, the drive amplitude is kept very small to keep the resonator in the linear response regime and to also ensure negligible background magnetic field that might affect measurements. In order to isolate the spring effect from the coupling effect, magnet 1 was mounted on the spring, while magnet 2 was fixed to an xyz stage resulting in $\theta_2, y_2 = 0$ [Fig. 4(e)]. Here onward, we refer to magnet 1 as the resonating magnet and magnet 2 as the fixed magnet. We first measured the unperturbed torsional mode resonance frequency (515 Hz) and the bending mode resonance frequency (370 Hz) of the isolated resonator to establish a baseline.

To test the magnetostatic spring effect, we measured the fractional shift of each resonance frequency in two cases: a *parallel* configuration ($z = y = 0$ and the magnets are only spaced in x) and a *series* configuration ($z = x = 0$ and the magnets are only spaced in y). For the torsional mode, we anticipate from (6) that the parallel configuration will result in a positive value of γ, producing a spring *softening* effect. In contrast, the series configuration should result in a negative value of γ, producing a spring *stiffening* effect. For the bending mode, we expect that λ will be positive for both the parallel and series configurations, implying a spring softening effect for both. The two magnets can also be arranged in *anti-parallel* and *anti-series* configurations by flipping one of the dipoles so that it points in $-\hat{y}$, thereby changing the sign of γ, λ.

Experimental measurements of the fractional frequency shift for the torsional mode are shown in Fig. 5. We find good agreement between the predicted and measured frequency shift in all four (parallel, anti-parallel, series, and anti-series) configurations.

The experimentally measured fractional frequency shift for the bending mode is shown in Fig. 6. We again find good agreement between the predicted and measured frequency shift for the parallel and anti-parallel configurations. However, in the series and anti-series configurations, the predicted frequency shift is noticeably greater than the measured shift, especially for small separation distances. Finite-element simulations using Ansys Maxwell solver revealed that this discrepancy is due to shape effects that are not captured by the point dipole model, which reduce the effective dipole moment. The magnetic translational resonance is more sensitive to these shape effects than the rotational resonance due to its stronger

dependence on the position of the dipole, as can be seen by comparing Figs. 2 and 3. This effect decreases with relative distance and ultimately becomes negligible at long distances where the magnets are well-approximated by a point dipole.

IV. Conclusion and Discussion

We have presented an analytic model describing magnetostatic spring and coupling effects that arise from the interaction of magnetized mechanical resonators. These magnetostatic effects can produce either softening or stiffening of the resonator's effective spring constant, depending on the dipole orientation and the ambient magnetic field distribution. We verified our analytic model with simple experimental tests for resonators undergoing either rotational or translational resonant motion. We additionally note that the magnetic spring effect is generally nonlinear and the linearized approximations we use here are only valid for low amplitudes of motion and small driving forces. This type of system can, therefore, offer a reconfigurable platform for the investigation of non-linear effects in arrays of coupled nonlinear resonators.

Acknowledgment

This work was supported in part by the U.S. Office of Naval Research Director of Research Early Career Grant under Grant N00014-16-1-2830, in part by the National Science Foundation Emerging Frontiers in Research and Innovation NewLAW Program under Grant EFMA-1627184, in part by the National Science Foundation Graduate Research Fellowship, and in part by the Zuckerman STEM Leadership Program.

References

[1] H. A. C. Tilmans and R. Legtenberg, "Electrostatically driven vacuum-encapsulated polysilicon resonators: Part II. Theory and performance," *Sens. Actuators A, Phys.*, vol. 45, no. 1, pp. 67–84, 1994. doi: 10.1016/0924-4247(94)00813-2.

[2] T. Veijola *et al.*, "Large-displacement modelling and simulation of micromechanical electrostatically driven resonators using the harmonic balance method," in *IEEE MTT-S Int. Microw. Symp. Dig.*, vol. 1, Jun. 2000, pp. 99–102.

[3] D. Rugar and P. Hansma, "Atomic force microscopy," *Phys. Today*, vol. 43, no. 10, pp. 23–30, 1990.

[4] F. J. Giessibl, "Advances in atomic force microscopy," *Rev. Modern Phys.*, vol. 75, no. 3, p. 949, Jul. 2003.

[5] A. Buonanno and Y. Chen, "Optical noise correlations and beating the standard quantum limit in advanced gravitational-wave detectors," *Classical Quantum Gravity*, vol. 18, no. 15, pp. L95–L101, 2001.

[6] B. S. Sheard, M. B. Gray, C. M. Mow-Lowry, D. E. McClelland, and S. E. Whitcomb, "Observation and characterization of an optical spring," *Phys. Rev. A, Gen. Phys.*, vol. 69, no. 5, 2004, Art. no. 051801.

[7] U. Hartmann, "Magnetic force microscopy," *Annu. Rev. Mater. Sci.*, vol. 29, pp. 53–87, Aug. 1999.

[8] H. Hopster and H. P. Oepen, *Magnetic Microscopy of Nanostructures*. Berlin, Germany: Springer, 2006.

[9] B. P. Mann and N. D. Sims, "Energy harvesting from the nonlinear oscillations of magnetic levitation," *J. Sound Vib.*, vol. 319, nos. 1–2, pp. 515–530, Jan. 2009.

[10] A. R. M. Foisal, C. Hong, and G.-S. Chung, "Multi-frequency electromagnetic energy harvester using a magnetic spring cantilever," *Sens. Actuators A, Phys.*, vol. 182, pp. 106–113, Aug. 2012.

[11] M. Han, Q. Yuan, X. Sun, and H. Zhang, "Design and fabrication of integrated magnetic MEMS energy harvester for low frequency applications," *J. Microelectromech. Syst.*, vol. 23, no. 1, pp. 204–212, Feb. 2014.

[12] A. L. Herrera-May, L. A. Aguilera-Cortés, P. Garciía-Ramírez, and E. Manjarrez, "Resonant magnetic field sensors based on MEMS technology," *Sensors*, vol. 9, no. 10, pp. 7785–7813, 2009.

[13] P. Pai, H. Pourzand, and M. Tabib-Azar, "Magnetically coupled resonators for rate integrating gyroscopes," in *Proc. IEEE Sensors*, Nov. 2014, pp. 1173–1176.

[14] L. Long, M. Wang, and S. Zhong, "A torsion MEMS magnetic sensor with permanent magnet and fiber-optic detection," *IEEE Sensors J.*, vol. 16, no. 23, pp. 8426–8433, Dec. 2016.

[15] K. Tsai *et al.*, "Magnetic, mechanical, and optical characterization of a magnetic nanoparticle-embedded polymer for microactuation," *J. Microelectromech. Syst.*, vol. 20, no. 1, pp. 65–72, 2011.

[16] X. Sun, Q. Yuan, D. Fang, and H. Zhang, "Electrodeposition and characterization of CoNiMnP permanent magnet arrays for MEMS sensors and actuators," *Sens. Actuators A, Physical*, vol. 188, pp. 190–197, Dec. 2012.

[17] G. Lemarquand, R. Ravaud, I. Shahosseini, V. Lemarquand, J. Moulin, and E. Lefeuvre, "MEMS electrodynamic loudspeakers for mobile phones," *Appl. Acoust.*, vol. 73, no. 4, pp. 379–385, 2012.

[18] J. A. Little, R. Carroll, M. J. Mazzoleni, N. Garraud, D. P. Arnold, and B. P. Mann, "Investigation of wave propagation behavior in magnetically coupled MEMS oscillators," in *Proc. ASME Int. Design Eng. Tech. Conf. Comput. Inf. Eng. Conf.*, Aug. 2015, Art. no. V004T09A016.

[19] R. E. Carroll, J. A. Little, B. P. Mann, and D. P. Arnold, "Demonstration of tunable energy propagation using magneto-mechanical oscillator arrays," in *Proc. IEEE 30th Int. Conf. Micro Electro Mech. Syst.*, Jan. 2017, pp. 873–876.

[20] L. M. Nash, D. Kleckner, A. Read, V. Vitelli, A. M. Turner, and W. T. Irvine, "Topological mechanics of gyroscopic metamaterials," *Proc. Nat. Acad. Sci.*, vol. 112, no. 47, pp. 14495–14500, Nov. 2015.

[21] K.-X. Qian, P. Zeng, W.-M. Ru, and H.-Y. Yuan, "Novel magnetic spring and magnetic bearing," *IEEE Trans. Magn.*, vol. 39, no. 1, pp. 559–561, Jan. 2003.

[22] J. Choi, S. Park, W. Lee, and S.-C. Kang, "Design of a robot joint with variable stiffness," in *Proc. IEEE Int. Conf. Robot. Autom.*, May 2008, pp. 1760–1765.

[23] A. Sudano, D. Accoto, L. Zollo, and E. Guglielmelli, "Design, development and scaling analysis of a variable stiffness magnetic torsion spring," *Int. J. Adv. Robotic Syst.*, vol. 10, no. 10, p. 372, Oct. 2013.

[24] H. Sarafian, "Nonlinear oscillations of a magneto static spring-mass," *J. Electromagn. Anal. Appl.*, vol. 3, no. 5, p. 133, May 2011.

[25] D. Vokoun, M. Beleggia, L. Heller, and P. Šittner, "Magnetostatic interactions and forces between cylindrical permanent magnets," *J. Magnetism Magn. Mater.*, vol. 321, no. 22, pp. 3758–3763, Nov. 2009.

[26] A. H. Memar and E. T. Esfahani, "A variable stiffness gripper with antagonistic magnetic springs for enhancing manipulation," in *Proc. Robot., Sci. Syst.*, Jun. 2018, p. 1–9.

[27] A. Sudano, N. L. Tagliamonte, D. Accoto, and E. Guglielmelli, "A resonant parallel elastic actuator for biorobotic applications," in *Proc. IEEE/RSJ Int. Conf. Intell. Robot. Syst.*, Sep. 2014, pp. 2815–2820.

[28] A. Nammari and H. Bardaweel, "Design enhancement and non-dimensional analysis of magnetically-levitated nonlinear vibration energy harvesters," *J. Intell. Mater. Syst. Struct.*, vol. 28, no. 19, pp. 2810–2822, Nov. 2017.